Available online at www.sciencedirect.com
ScienceDirect
Journal of Power Sources 174 (2007) 770–773
JOURNAL OF POWER SOURCES
www.elsevier.com/locate/jpowsour

Short communication

Nanosized tin anode prepared by laser-induced vapor deposition for lithium ion battery

T. Zhang [a], L.J. Fu [a], J. Gao [a], Y.P. Wu [a,b,*], R. Holze [b,**], H.Q. Wu [a]

[a] *Department of Chemistry & Shanghai Key Laboratory of Molecular Catalysis and Innovative Materials, Fudan University, Shanghai 200433, China*
[b] *Institut für Chemie, AG Elektrochemie, Technische Universität Chemnitz, D-09111 Chemnitz, Germany*

Available online 3 July 2007

Abstract

Nanosized tin powder was prepared by laser-induced vapor deposition and studied as an alternative anode material for lithium ion batteries. The nano tin particles are spherical, and their size varies from 5 nm to 80 nm. The prepared powder consists of two compounds: a major amount of Sn and a minor amount of SnO. Results of cyclic voltammograms (CVs) indicate that SnO is deoxidized to Sn almost completely in the first cycle. The reaction of tin with lithium proceeds in two steps. At first, a Li-deficient phase is formed, later a Li-rich phase. Reaction kinetics are controlled by a diffusion step, and the diffusion coefficient of lithium ions in the anode is calculated to be 4.15×10^{-8} cm^2 s^{-1}. The initial charge capacity is nearly to the theoretical reversible capacity of lithium insertion into tin, resulting in $Li_{22}Sn_5$.

Keywords: Lithium ion battery; Nanosized Sn; Anode; Laser-induced vapor deposition

1. Introduction

Lithium ion batteries are required to improve their capacity and cycleability obviously because of their rapid advances in the fields of portable PCs, cellular phones, digital cameras, military electronic equipment, and environmentally benign electric vehicles (EVs), etc. Latest research in anode materials for lithium ion battery is focused on finding new materials with high capacity and excellent cycling behavior and on synthetic methods to replace the conventional carbon-based anode materials [1–4].

Recently, alloys were extensively studied because of their high specific gravimetric and volumetric capacities (e.g., Li/Sn: 990 mAh g^{-1}, Li/Sb: 660 mAh g^{-1}) [5,6]. However, none of the alloy systems has been commercialized mainly because of the poor integrity of the materials during Li+ intercalation and de-intercalation. The large volume change during charge and discharge generates severe mechanical stress which results in pulverization and exfoliation of the particles. This deterioration causes loss of electrical contact of Li-alloy material, which gives rise to poor cycling stability. To overcome this problem, intermetallic compounds [7,8], active/inactive nanocomposite materials [9,10], and thin film materials [11,12] have been studied. It is found that small absolute volume changes occurring for nanomaterials due to their small particle size and uniform particle distribution can mitigate the pulverization of the particles and lead to slow capacity fade.

In this study, we prepared tin nanoparticles by a laser-induced vapor deposition method and investigated its electrochemical performance and kinetic parameter as anode material for Li ion battery.

2. Experimental

High purity tin powder was placed in a vacuum chamber. The chamber was pumped down to a pressure below 10 Pa and subsequently filled with Ar gas up to 5 kPa. Induction heating was applied to melt the tin powder. The melt was illuminated with a laser and quickly evaporated. The atomized tin condensed onto the water-cooled wall of the chamber generating tin nanoparticles.

Two-electrode coin-type half-cells were assembled for the evaluation of electrochemical performance. Nano tin powder (64% by mass) was mixed with 16% acetylene black (AB)

* Corresponding author at: Department of Chemistry & Shanghai Key Laboratory of Molecular Catalysis and Innovative Materials, Fudan University, Shanghai 200433, China.
** Corresponding author.
E-mail addresses: wuyp@fudan.edu.cn (Y.P. Wu), rudolf.holze@chemie.tu-chemnitz.de (R. Holze).

0378-7753/$ – see front matter © 2007 Published by Elsevier B.V.
doi:10.1016/j.jpowsour.2007.06.231

as conductive additive and 20% poly(vinylidene fluoride) as binder. *N*-Methyl-pyrrolidone was used as solvent. The slurry was coated on copper foil. After drying, it was cut into round discs with a diameter of about 1 cm and about 10 mg weight. Using these pellets as working electrode, coin-type model cells were assembled in a glove box filled with argon. Li metal was used as the counter and reference electrode, Celgard 2400 as the separator, and a 1 mol l^{-1} $LiPF_6$ in diethylcarbonate (DEC)/ethylenecarbonate (EC)/dimethylcarbonate (DMC) (1:1:1 by mass) solution as the electrolyte. Cycle testing of the coin-type half-cells was performed in the voltage range 0.01–2 V with a constant current density 0.2 mA cm^{-2} at room temperature (Land 2001A). Cyclic voltammograms (CV) were measured in the range of 0–2.0 V at scanning rates of 0.1, 0.2, 0.3, 0.4 and 0.5 mV s^{-1}, respectively.

X-ray diffraction (XRD) pattern were obtained with Cu Kα radiation on a Rigaku RINT-2000 diffractometer. TEM was performed with a transmission electron microscope JEOL JEM 2011. SEM was performed with a scanning electron microscope Philips XL300.

3. Results and discussion

The XRD pattern of tin powder prepared by laser-induced vapor deposition method is shown in Fig. 1. It can be seen that the powder consists of two components: a major amount of crystalline tin and a small amount of SnO crystal. SnO is perhaps formed by oxidation of Sn during exposure of the nano Sn particles to the ambient environment due to large reactivity of nano tin with oxygen and water in air.

Fig. 2(a) is the SEM micrograph of the tin powder. It shows that the size of the tin powder particles is on the nanoscale. Furthermore, the TEM micrograph of the Sn particles shows their spherical morphology, the particle size varies from 5 nm to 80 nm. Although the particle size is not uniform, all nano particles disperse homogeneously and do not aggregate together.

Fig. 3 shows cyclic voltammograms (CVs) of the tin anode measured between 0 V and 2.0 V at a scanning rate of 0.5 mV s^{-1} during the first, second and fifth scans. In the first reduction half-cycle, the CV curve begins to decline at about 1.1 V, which corresponds to the formation of the solid electrolyte interface (SEI) film on the surface of the active particles. Later, an apparently irreversible reduction peak appears at 0.7 V versus Li/Li+,

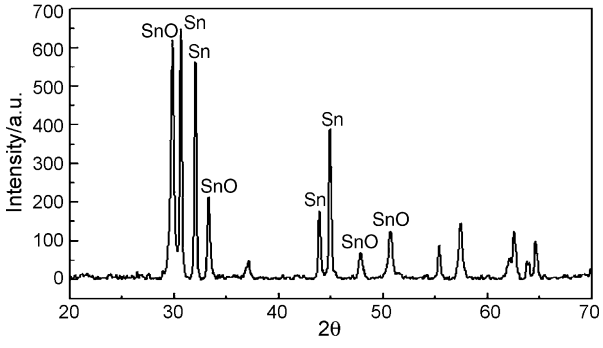

Fig. 1. XRD pattern of the laser-induced chemical vapor deposition Sn powder.

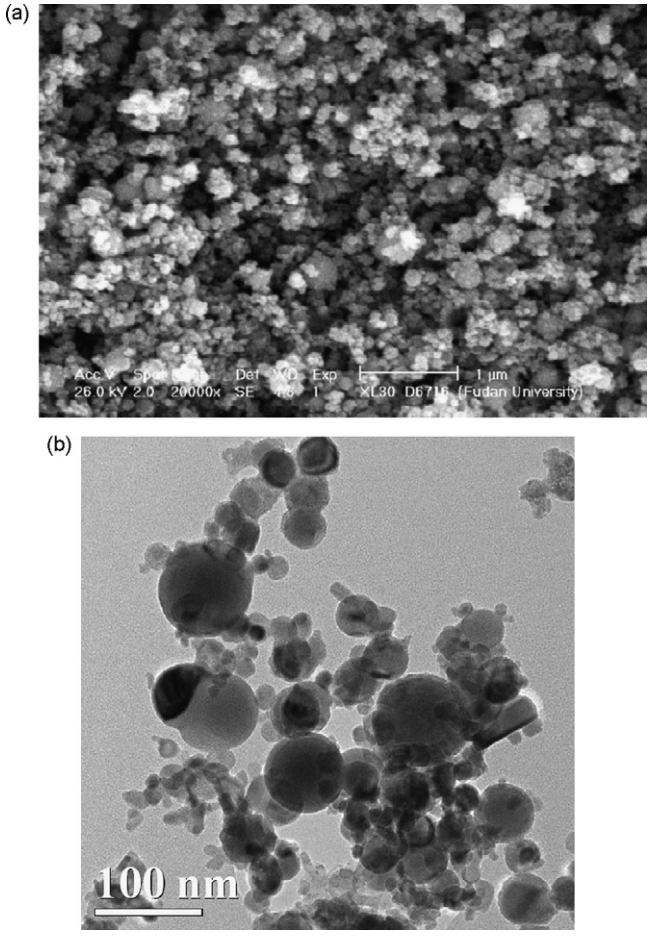

Fig. 2. (a) TEM micrograph and (b) SEM micrograph of the laser-induced chemical vapor deposition Sn powder.

which is related to the reduction of SnO to metallic Sn and $2Li_2O$ [13,14]. Owing to the large surface area of the nanoparticles, this reduction process overlaps partially with the broad formation process of the SEI film, leading to mostly irreversible capacity in the first cycle together. This SnO-reduction peak disappears in the following cycles, indicating that SnO has been reduced

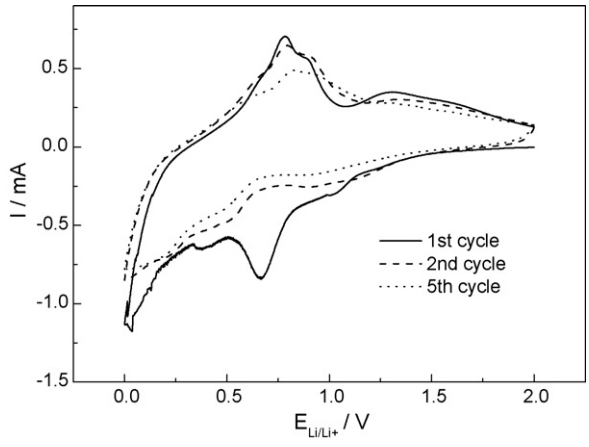

Fig. 3. Cyclic voltammograms of laser-induced chemical vapor deposition Sn anode measured at the range of 0–2.0 V with a scanning rate of 0.5 mV s^{-1} during the first, second and fifth cycles.

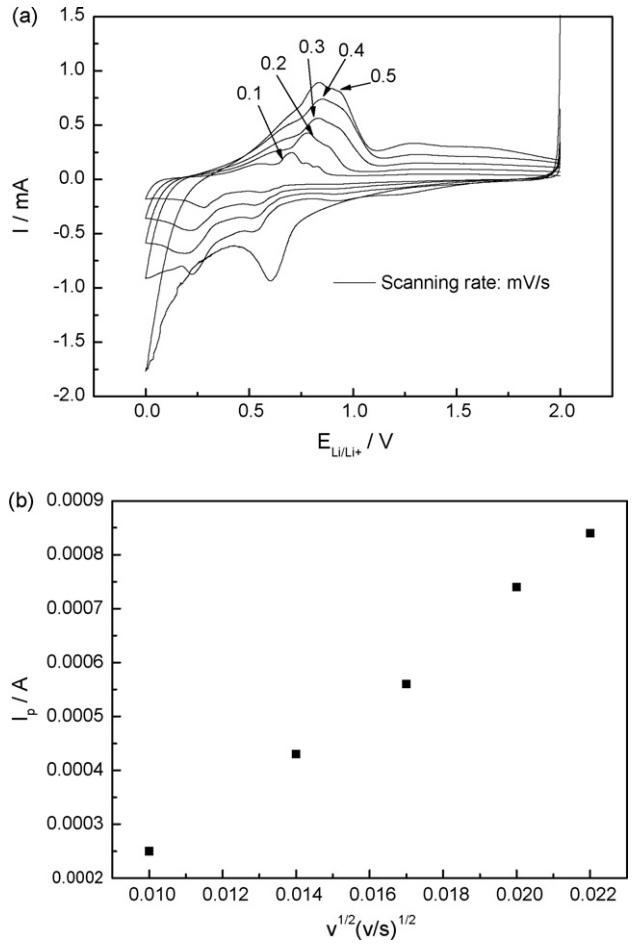

Fig. 4. (a) Cyclic voltammograms of nano Sn anode measured at the range of 0–2.0 V with different scanning rate and (b) the relationship between I_p and $v^{1/2}$.

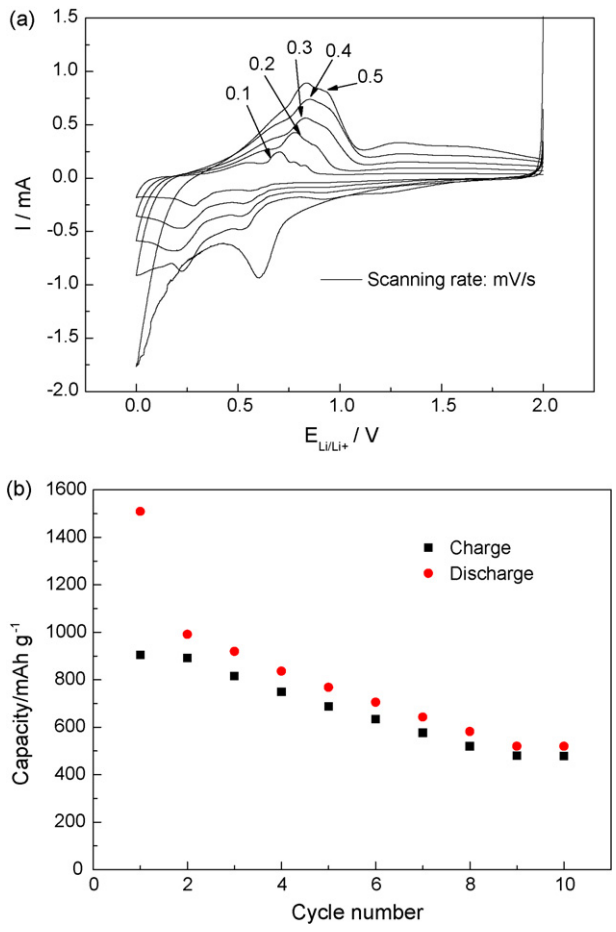

Fig. 5. Electrochemical performance of the laser-induced chemical vapor deposition Sn anode cycled between 0.01 V and 2.0 V with a constant current of 0.2 mA cm^{-2}: (a) the charge/discharge profiles; (b) the cycling behavior.

completely to Sn in the first cycle. The shape of cyclic votammograms is stable with scanning. The current peaks at 0.5 V and 0.3 V in the reduction process are caused by the formation of Li–Sn alloys. According to Huggins' report, these two peaks are related to the formation of a Li-deficient phase (0.5 V) and a Li-rich phase (0.3 V) [15].

The CVs at different scan rates reveal further interesting phenomena (see Fig. 4(a)). We found that the oxidation peak current at different scan rate is proportional to the root of the scan rate, $v^{1/2}$, indicating that the reaction kinetics is controlled by the diffusion step. Moreover, based on the CV data at different scan rates and the following equation [16]:

$$I_p = 2.69 \times 10^5 A n^{3/2} C_0 D^{1/2} v^{1/2} \quad (1)$$

where n is the number of electrons per molecule during the intercalation, A the surface area of the anode, C_0 the concentration of lithium ions, D the diffusion coefficient of lithium ion, and v is the scan rate a linear relationship between I_p and $v^{1/2}$ was obtained as shown in Fig. 4(b). The diffusion coefficient of lithium ions in the tin anode is calculated to be 4.15×10^{-8} cm^2 s^{-1}. This diffusion coefficient is three times larger than that for Li^+ diffusing into silicon (1.47×10^{-8} cm^2 s^{-1}), suggesting that the nano anode has superior C-rate charging and discharging behavior [17].

Fig. 5(a) shows the charge and discharge profiles of the tin electrode in 1 mol l^{-1} $LiPF_6$ DEC/EC/DMC (w/w/w = 1/1/1) during the first, second and fifth cycles, respectively. The theoretical reversible capacity of lithium insertion into Sn forming $Li_{22}Sn_5$ is 990 mAh g^{-1}. The charge capacity in the first cycle is 904.4 mAh g^{-1}, almost equal to the theoretical capacity, which indicates that the $Li_{22}Sn_5$ alloy phase is formed. It can be speculated that the high initial capacity is due to the nanosize and fine dispersion of the Sn nanoparticles. It is found that the capacity loss of the Sn-based alloys occurs in the initial cycles especially during the first lithiation process. In the case of this nano tin material, the capacity loss in the first lithiation process is mainly due to the deoxidation of SnO. The similarity between the first and the second charge curve suggests that the small particle size and uniform particle distribution suppress pulverization of the tin particles. However, the difference between the second and the fifth curve shows that there is structural transformation occurring during cycling. As illustrated by the cycling behavior of the tin anode in Fig. 5(b), after 10 cycles the charge capacity fades quickly to 478.9 mAh g^{-1}, only half of the original capacity. The reason of this capacity decline is the mobility of the nanosized tin particles leading to aggregation into larger tin particles as the cycle number increases. Larger tin particles are

more sensitive to cracking and crumbling due to larger absolute volume changes than smaller particles [9]. We have synthesized a core-shell TiO_2/C and Si/C nanocomposite by emulsion polymerization and subsequent heat-carbonization process. The carbon shell acts as a barrier suppressing the aggregation of TiO_2 and Si nanoparticles thus increasing their structural stability during cycling. Consequently, the capacity retention of the TiO_2 and Si nanoparticles is improved [16,18]. It is obvious that the same method can be utilized to enhance the cycle performance of nanosized tin particles. We will try to clarify this point in following studies.

4. Conclusion

A nanosized tin powder prepared by laser-induced vapor deposition has been studied as anode material for lithium ion battery. The reaction of tin with lithium proceeds in two steps: first into a Li-deficient phase and latter into a Li-rich phase. The reaction kinetic is controlled by the diffusion step. The diffusion coefficient of lithium ions in the tin anode is calculated to be $4.15 \times 10^{-8}\,cm^2\,s^{-1}$ suggesting that the nano tin anode has superior C-rate charging and discharging behavior. The initial charge capacity is high, close to the theoretical reversible capacity of lithium insertion into tin, mainly because of the fine dispersion of the Sn nanoparticles.

Acknowledgements

Financial supports from National Basic Research Program of China (973 Program No:2007CB209700), Shanghai Science & Technology Committee (0552nm05025 and 04QMX1406), China Natural Science Foundation (20474010) and Alexander von Humboldt Foundation are greatly appreciated.

References

[1] Y.P. Wu, X.B. Dai, J.Q. Ma, Y.J. Chen, Lithium Ion Battery: Applications & Practice, Chemical Industry Press, Beijing, 2004, pp. 99–101.
[2] Y. Wang, J.Y. Lee, J. Phys. Chem. B 108 (2004) 17832.
[3] N. Perira, L. Duppont, J.M. Trarscon, L.C. Klein, G.G. Amatucci, J. Electrochem. Soc. 150 (2003) A1272.
[4] L.J. Fu, H. Liu, Y.P. Wu, E. Rahm, R. Holze, H.Q. Wu, Prog. Mater. Sci. 50 (2005) 881.
[5] I. Rom, M. Wachtler, I. Papst, M. Schmied, J.O. Besenhard, F. Hofer, M. Winter, Solid State Ionics 143 (1999) 329.
[6] M.M. Thackeray, J.T. Vaughey, C.S. Johnson, A.J. Kropf, R. Benedek, L.M.L. Fransson, E. Edstron, J. Power Sources 113 (2003) 124.
[7] Y.U. Kim, C.K. Lee, H.J. Sohn, T. Kanga, J. Electrochem. Soc. 151 (2004) A933.
[8] J. Xie, G.S. Cao, X.B. Zhao, Y.D. Zhong, M.J. Zhao, J. Electrochem. Soc. 151 (2004) A1905.
[9] D.G. Kim, H. Kim, H.J. Sohn, T. Kang, J. Power Sources 104 (2002) 221–225.
[10] J. Wolfenstine, S. Campos, D. Foster, J. Read, W.K. Behl, J. Power Sources 109 (2002) 230.
[11] H. Mukaibo, T. Sumi, T. Yokoshima, T. Momma, T. Osaka, Electrochem. Solid-State Lett. 6 (2003) A218.
[12] W. Choi, J.Y. Lee, H.S. Lim, Electrochem. Commun. 6 (2004) 816.
[13] I. Grigoriants, A. Soffer, G. Salitra, D. Aurbach, J. Power Sources 146 (2005) 185.
[14] Y.L. Zhang, Y. Liu, M.L. Liu, Chem. Mater. 18 (2006) 4643.
[15] R.A. Huggins, J. Power Sources 81/82 (1999) 13–19.
[16] J. Graetz, C.C. Ahn, R. Yazami, B. Fultz, J. Electrochem. Soc. 151 (2004) A698.
[17] L.J. Fu, H. Liu, H.P. Zhang, C. Li, T. Zhang, Y.P. Wu, R. Holze, H.Q. Wu, Electrochem. Commun. 8 (2006) 1.
[18] T. Zhang, L.J. Fu, J. Gao, L.C. Yang, Y.P. Wu, H.Q. Wu, Pure Appl. Chem. 78 (2006) 1889.